Journal of Power Sources 342 (2017) 956–963

Contents lists available at ScienceDirect

Journal of Power Sources

journal homepage: www.elsevier.com/locate/jpowsour

Improved electrical power production of thermally regenerative batteries using a poly(phenylene oxide) based anion exchange membrane

Mohammad Rahimi [a], Liang Zhu [b], Kelly L. Kowalski [a], Xiuping Zhu [c, d], Christopher A. Gorski [c], Michael A. Hickner [a, b, e], Bruce E. Logan [c, *]

[a] Department of Chemical Engineering, The Pennsylvania State University, University Park, PA 16802, USA
[b] Department of Materials Science and Engineering, The Pennsylvania State University, University Park, PA 16802, USA
[c] Department of Civil and Environmental Engineering, The Pennsylvania State University, University Park, PA 16802, USA
[d] Department of Civil and Environmental Engineering, Louisiana State University, Baton Rouge, LA 70803, USA
[e] Department of Chemistry, The Pennsylvania State University, University Park, PA 16802, USA

HIGHLIGHTS

- A battery based on ammonia and copper salts was used to produce electricity.
- Quaternary ammonium-based poly(-phenylene oxide) membranes were tested.
- The synthesized membranes had different ion exchange capacities and thicknesses.
- The power density of the BTMA membrane (40% DF, 50 μm thick) was 106 ± 7 W m^{-2}.
- Energy recovery was estimated to reach 7.0% relative to the Carnot efficiency.

GRAPHICAL ABSTRACT

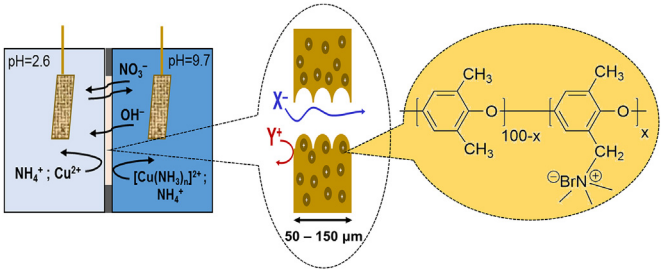

ARTICLE INFO

Article history:
Received 12 November 2016
Received in revised form
15 December 2016
Accepted 1 January 2017

Keywords:
Waste heat
Thermally regenerative battery
Anion exchange membrane
Energy harvesting
Thermal efficiency

ABSTRACT

Thermally regenerative ammonia-based batteries (TRABs) can be used to harvest low-grade waste heat as electrical power. To improve TRAB performance, a series of benzyltrimethyl quaternary ammonium-functionalized poly(phenylene oxide) anion exchange membranes (BTMA-AEMs) were examined for their impact on performance relative to a commercial AEM (Selemion AMV). The synthesized AEMs had different degrees of functionalization (DF; 25% and 40%), and thicknesses (50, 100 and 150 μm). Power and energy densities were shown to be a function of both DF and membrane thickness. The power density of TRAB increased by 31% using a BTMA-AEM (40% DF, 50 μm thick; 106 ± 7 W m^{-2}) compared to the Selemion (81 ± 5 W m^{-2}). Moreover, the energy density increased by 13% when using a BTMA-based membrane (25% DF, 150 μm thick; 350 Wh m^{-3}) compared to the Selemion membrane (311 Wh m^{-3}). The thermal-electric conversion efficiency improved to 0.97% with the new membrane compared to 0.86% for the Selemion. This energy recovery was 7.0% relative to the Carnot efficiency, which was 1.8

* Corresponding author.
E-mail address: blogan@psu.edu (B.E. Logan).

http://dx.doi.org/10.1016/j.jpowsour.2017.01.003

times greater than the highest previously reported value of a system used to capture low-grade waste heat as electricity.

1. Introduction

A significant amount of low-grade waste heat (temperature < 130 °C), approximately half of the current U.S.A energy demand (2.9×10^{13} kWh in 2013), is generated at industrial plants in the U.S. [1–4]. In recent years, harvesting low-grade waste heat as electrical power has drawn increasing attention due to its vast potential and availability often at locations where electrical power is needed [5–8]. One method of direct waste-heat-to-electricity energy conversion is solid-state thermoelectrics based on p- and n-type semiconductor materials [9–11], but high costs, long-term unreliability, and lack of capacity for energy storage have limited applications of these technologies [11]. Liquid-based thermoelectrochemical cells (TECs) that utilize the temperature dependence of electrochemical redox potentials to drive an electrochemical cell offer an alternative, potentially less expensive and scalable system for direct thermal-electric energy conversion, with opportunities for energy storage [12–14]. While a considerable amount of progress has been achieved during recent years in developing new types of TECs, their power densities and thermal-electricity energy conversion efficiencies need to be improved to make them commercially viable [15].

A thermally regenerative ammonia battery (TRAB) was recently developed as a new approach to harvest low-grade waste heat as electrical power that improved power densities compared to existing TECs [16]. In a TRAB, two copper electrodes are exposed to a copper(II) electrolyte, such as copper(II) nitrate. The two electrode chambers are separated by a membrane, as discussed below. Electrical power is produced by adding ammonia to the anolyte, but not to the catholyte (Fig. S1a). The ammonia complexes copper(II) and generates a potential difference between the electrodes according to the following reactions:

$$Cu^{2+}_{(aq)} + 2e^- \rightarrow Cu_{(s)}\ ;\ E^0 = +0.340\ V \quad (1)$$

$$Cu_{(s)} + 4NH_{3\ (aq)} \rightarrow CU(NH_3)^{2+}_{4\ (aq)} + 2e^-;\ E^0 = -0.04\ V \quad (2)$$

where E^0 is the standard reduction potential vs. the standard hydrogen electrode (SHE) [17]. After discharging the cell (Fig. S1b), ammonia is separated from the anolyte using conventional separation technologies, such as distillation, that utilize low-grade waste heat (Fig. S1c) [18,19]. The distilled ammonia is then added to the other electrolyte chamber for the next discharge cycle (Fig. S1d). By switching the compartment that contains ammonia, copper is re-deposited onto the formerly dissolved electrode, and the other electrode dissolves (Fig. S1e). This alternating cycle of electrode dissolution/deposition allows the Cu electrodes to be maintained in closed-loop cycles, and waste heat energy is converted to electricity through ammonia distillation (Fig. S2). A maximum power density of 80 W m^{-2}-electrode area with a thermal-electricity conversion efficiency of 0.86% (6.2% relative to the Carnot efficiency), has been achieved using a TRAB containing a commercial anion exchange membrane (AEM) [16,19,20].

In a TRAB, an AEM is used to separate the cathode and anode compartments and facilitate ion conduction to balance the internal charge transfer through transport of anions such as nitrate and hydroxide between the electrolyte chambers. In addition, the AEM minimizes self-discharge by reducing the transfer of either ammonia or positively-charged copper(II) amine complexes from the anolyte to the catholyte, and copper(II) ions from the catholyte to the anolyte (Fig. 1a). However, the transfer of hydroxide from the alkaline anode chamber (pH = 9.7) to the acidic cathode chamber (pH = 2.6) results in a shift in the NH_4^+/NH_3 acid/base equilibrium towards NH_3 formation in the cathode chamber (Eq. S(1)). This formation of NH_3 in the cathode chamber results in an unfavorable chemical consumption (Eqs. S2–S5) instead of electrochemical consumption of copper ions (Eq. (1); Fig. 1b). In previous TRAB tests using a commercial AEM (Selemion AMV), substantial self-discharge occurred that limited the electrical energy production [16,20]. In addition, in our recent study on copper removal from water using an adaption of a TRAB, it was shown that the cell self-discharge limited the effectiveness of copper removal at low initial concentrations of copper in the catholyte (<0.01 M) [21].

Here, we hypothesized that by varying the AEM's thickness and ion exchange capacity (IEC), we could reduce cell self-discharge and

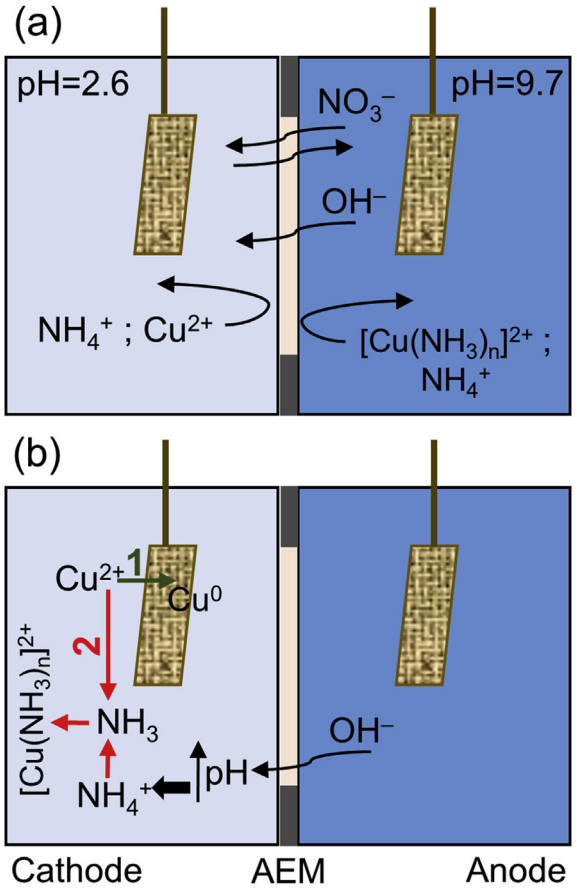

Fig. 1. Schematic of the TRAB with an anion exchange membrane (AEM): (a) AEM prevents transfer of both NH_3 and positively charged species, (b) higher transfer of OH^- through the membrane causes a higher rate of TRAB self-discharge by chemical consumption of copper ions (reaction 2; $Cu^{2+} + n\ NH_3 \rightarrow Cu(NH_3)^{2+}_n$).

maximize energy production. To test this hypothesis, anion exchange membranes were synthesized using poly(phenylene oxide) (PPO) backbones with pendant benzyltrimethyl ammonium cations (BTMA). These types of membranes were previously shown to be more efficient, potentially less expensive, and more chemically and thermally stable than commercially available membranes [22–26]. The performance of these PPO-based AEMs were evaluated in a TRAB cell in terms of power density, membrane resistance, energy density, cell self-discharge, and thermal-electricity efficiency based on comparisons to the AEM used in previous research (Selemion AMV). Since AEMs in TRAB are exposed to solutions that have low pH (2.6 for the cathode) or high pH (9.7 for the anode), the stabilities of the fabricated membranes were examined in strongly acidic or alkaline solutions.

2. Experimental section

2.1. Membrane preparation

Brominated PPO polymers, having a degree of functionalization (DF) of 25 and 40 mol % of the repeat units on the backbone with one benzyl bromide group (Br-PPOx; x = 25 or 40) were synthesized as previously described [27,28]. The molecular weight of PPO was 30000 g mol^{-1}, while that of brominated PPO was 39000 g mol^{-1}. Brominated PPO with a DB of 40% (Br-PPO40; 2.0 g) was dissolved in 20 mL of N-methyl-pyrrolidone (NMP; 97%; Sigma-Aldrich), and 3.2 mL of aqueous trimethylamine (~45 wt %; ≥99%; Sigma-Aldrich). The mixture was stirred for 24 h at room temperature, and poured into 100 mL of toluene (99.8%; Sigma-Aldrich) or hexane (95%; Sigma-Aldrich) to precipitate the polymer. The product was filtered and washed with toluene or hexane several times. The dark yellow mixture which was produced with a yield of 87% was dried at 50 °C overnight under vacuum. The formed powder (2 g) was then dissolved in NMP (20 mL), and an appropriate amount of the solution, depending on the membrane final thickness, was cast onto a leveled glass plate. The cast solution was dried at 82 °C under ambient pressure for 24 h followed by vacuum drying for another 24 h at 80 °C to obtain a B40-y membrane, where B40 refers to the degree of functionalization of a BTMA-based membrane and *y* stands for the membrane thickness (Fig. S3). All other Bx-y membranes were prepared using similar procedures as described above.

In order to remove the solvent from the polymer during the membrane preparation, samples were dried at various temperatures to the point at which the mass of the polymers or membranes were constant. The drying temperatures depend on the specific solvents which were used. For the low boiling point solvents such as hexanes and toluene, lower drying temperatures (50 °C, 60 °C) were sufficient to remove the solvents under vacuum. To remove NMP which has a higher boiling point, a higher drying temperature (80 °C) was employed under vacuum.

2.2. Membrane characterization and measurements

To identify the membrane structure, ^{1}H NMR spectra were recorded at 300 MHz on a spectrometer (AV 300, Bruker, Billerica, MA) using DMSO-d_6 as the solvent. Water uptake was measured after drying the membrane at 60 °C under vacuum for 24 h. The dried membrane was immersed in water and periodically weighed on an analytical balance until a constant mass was obtained, giving the mass-based water uptake. Water uptake (WU) was calculated as $WU = (m_{hyd} - m_0)/m_0$, where m_{hyd} is the hydrated sample mass and m_0 is the dry sample mass. To calculate the titrated gravimetric IEC values, membranes in the OH^- form were immersed in 50 mL of 0.01 M HCl standard solution for 24 h. Then, the solutions were titrated with a standardized NaOH (0.01 M) solution to pH = 7. Subsequently, the samples were washed and immersed in deionized water for 24 h to remove the residual HCl, and then dried under vacuum at 50 °C overnight and weighed to calculate the dry masses in the Cl^- form. The IEC of the membranes was calculated as:

$$IEC = \frac{n_{i(H^+)} - n_{f(H^+)}}{m_{dry(Cl)}} \quad (3)$$

where $m_{dry(Cl)}$ is the mass of dry membranes, $n_{i(H^+)}$ is the initial amount of H^+ in the HCl solution, $n_{f(H^+)}$ is the final amount of H^+ in the HCl solution.

Electrochemical impedance spectroscopy (EIS; VMP3, Bio-Logic) was used to quantify different components of the resistances of the various membranes in the TRAB system. All EIS experiments were measured over a frequency range of 100 kHz to 0.1 Hz with a sinusoidal amplitude of 10 mV. The batteries were discharged at 0.2 V for 5 min with stable current production before imposing a sinusoidal perturbation to achieve a pseudo steady state. The EIS spectra were fitted into a simplified Randles equivalent circuit to identify the membrane resistance (Fig. S4; Eqs. S6 and S7).

Since the membrane in the TRAB was continuously in contact with acidic (catholyte pH = 2.6) and alkaline (anolyte pH = 9.7) solutions, the stabilities of the fabricated membranes were separately tested in acidic or alkaline conditions. Two membranes (B24 and B40) were immersed in solutions similar to that of the catholyte (0.1 M $Cu(NO_3)_2$, 5 M NH_4NO_3) or anolyte (0.1 M $Cu(NO_3)_2$, 5 M NH_4NO_3, 2 M NH_3) for a period of time (50 h) chosen to match about 30 cycles of the battery discharge, at room temperature. The membranes were then soaked in deionized water for 24 h, and then their performance was examined based on polarization tests. The durability of the fabricated membranes was also tested to evaluate the dry form stability after long-term storage. Membranes were stored dry for 1 year in a constant temperature room (30 °C), and then their performance was compared to newly fabricated membranes with the same IEC and thickness.

2.3. TRAB construction and operation

The TRAB was constructed as previously described [16,20]. The battery consisted of a cathode and an anode chamber, each 4 cm long and 3 cm in diameter, separated by an AEM (either Selemion AMV with a thickness of 100 μm, Asashi Glass, Japan; or the fabricated membranes) with a projected surface area of 7 cm^{-2}. Two 0.8 cm × 2 cm pieces of copper mesh (50 × 50 mesh; McMaster-Carr, OH) connected by copper wire were used as the electrodes. To monitor the electrode potentials, Ag/AgCl reference electrodes (+0.211 V vs. SHE; RE-5B; BASi) were inserted 1 cm away from each electrode (2 cm away from the membrane). The catholyte was mixed using a magnetic stirrer (6.4 × 15.9 mm; VWR) at 600 rpm.

The electrolytes were prepared by making a 0.1 M of $Cu(NO_3)_2$ (Sigma-Aldrich) solution with 5 M NH_4NO_3 as the supporting electrolyte to increase conductivity. Ammonium hydroxide (2 M final concentration; 5 N solution, Sigma-Aldrich) was added only to the anolyte to form the copper ammonia complex and create a potential difference between the cathode and anode chambers.

2.4. TRAB performance evaluation

Polarization measurements were performed using a data acquisition system (Agilent 34972A, Santa Clara, CA) to measure the cell voltage (*U*), and each electrode potential at room temperature. External resistances were switched every 3 min from open circuit

to 1.4 Ω in decreasing order (i.e. 21.4 Ω, 11.5 Ω, 6.4 Ω, 4.4 Ω, 3.4 Ω, 2.5 Ω, 1.4 Ω; total 24 min). Both current density ($i = U/RA$, A m^{-2}; i: current density, U = voltage, R = external resistance, and A = surface area), and power density ($P = U^2/RA$, W m^{-2}) were normalized using a single electrode projected surface area (1.6 cm^2) [29]. For discharge tests, the cell was operated with a fixed external resistance that produced the highest power (based on the polarization data), until the cell voltage decreased to 10 mV. Using the discharge test data, the energy density, normalized to the total electrolyte volume (E, Wh m^{-3}), was calculated as $E = \int UIt/V_t$, where U is the voltage (V), I the current (A), t the cycle time (h), and V_t the volume of the reactor (56 mL; 2 chambers with 28 mL each).

Copper electrochemical consumption (*CEC*) tests were performed to identify the fraction of Cu^{2+} deposition ($Cu^{2+} \rightarrow Cu^0$) that was due to the electrochemical reaction relative to the total amount of Cu^{2+} depletion (due to electrochemical and chemical reactions):

$$CEC\ (\%) = \frac{\left(m_f - m_0\right)}{C_i\, M\, V_c} \times 100 \quad (4)$$

where m_0 and m_f are electrode masses before and after the discharge test, C_i is the initial concentration of Cu^{2+} in the catholyte (0.1 M), M is the molecular weight of copper (63.55 g mol^{-1}), and V_c is the volume of cathode chamber (28 mL). Cathodic coulombic efficiency (*CCE*) was calculated as the ratio between actual produced charge to the theoretical charge based on the mass change of the electrode to find the dominant electrochemical reaction in the catholyte, as:

$$CCE\ (\%) = \frac{\left(m_f - m_0\right)}{\frac{Q}{2}\frac{M}{F}} \times 100 \quad (5)$$

where Q is the total charge transferred ($Q = \int It$, C), and F is Faraday's constant (96485 C mol^{-1}). For the cathode electrode, the mass was measured using an analytical balance with a precision of 0.0001 g, and the value was used for either the *CEC* or *CCE* calculations.

After discharging the TRAB, the battery was recharged by separating ammonia from the anolyte and re-dissolving it in the catholyte (Fig. S1c, d). In practice, low-grade waste heat (<130 °C) could be used for this process, for example by using a distillation column with a reboiler temperature of 70.4 °C and a condenser temperature of 43.3 °C (Fig. S2). Previous simulation results indicated that 97% of ammonia could be recovered during the designed separation process [16,20]. The thermal energy efficiency (η) was calculated as the ratio between the discharge energy and the required thermal energy for electrolyte regeneration (η = actual discharge energy/required thermal energy).

3. Results and discussion

3.1. Membrane characterization

The polymer structure of the fabricated BTMA-based AEMs was characterized by ^{1}H NMR spectroscopy. The peaks at 3.1 and 4.4 ppm for benzyltrimethylammonium indicated that the quaternary ammonium group was successfully formed (Fig. 2) [24]. Using ^{1}H NMR spectroscopy, it was also confirmed that the purity of the synthesized polymer was higher than 97%. The IEC of Selemion was 1.93 mmol g^{-1} which was similar to the previously reported value (~1.9 mmol g^{-1}) (Table 1) [30,31]. Raising the degree of functionalization from 25% (B25) to 40% (B40) increased the IEC from 1.82 to 2.04 mmol g^{-1}. This result was in agreement with the previous investigations which indicated that measured IEC is a function of

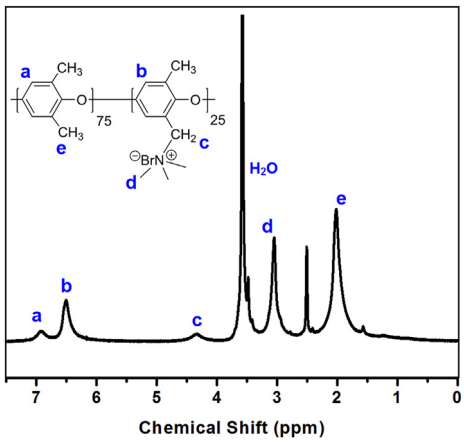

Fig. 2. ^{1}H NMR of B25 in DMSO-d_6/D_2O (10:1 wt:wt).

Table 1
IEC and water uptake of the Selemion compared to that of the B25 and B40 AEMs, all with a thickness of 100 μm.

Sample	IEC (mmol g^{-1})	Water uptake (wt %)
Selemion	1.93	20 ± 2
B25	1.82	63 ± 4
B40	2.04	80 ± 7

polymer functionalization degree [24,32,33]. The water uptake measured for the Selemion AMV (20 wt %) was significantly lower than that of the fabricated membranes (63% for B25; 80% for B40). Although the exact structure of the Selemion is not available, it is likely that either the functionalized head group or the polymer backbone of the Selemion was less hydrophilic than that of the BTMA-based AEM. Water uptake increased with the IEC, mainly because the benzyltrimethyl ammonium group on the polymer backbone enhanced the hydrophilicity of the fabricated membrane [33,34].

Membranes were analyzed by EIS to compare their operational resistances. The resistance decreased with an increase in IEC. For example, for the 100 μm thick membranes the resistance was 1.61 Ω for the B25-100 with an IEC of 1.82 mmol g^{-1}, and 1.14 Ω for B40-100 which had a higher IEC of 2.04 mmol g^{-1} (Fig. 3). In general, the membranes showed the expected trend that the resistance

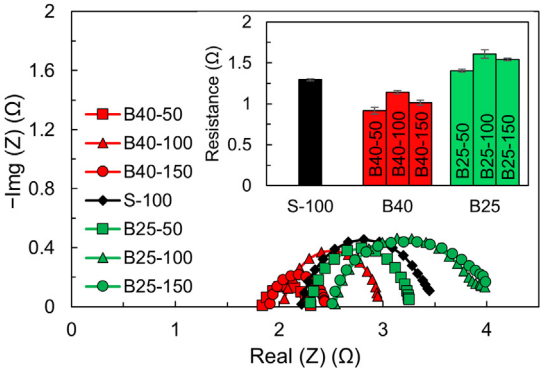

Fig. 3. Nyquist plots of the whole cell impedance at 0.2 V. The inserted figure indicates the membrane resistance obtained by fitting the Nyquist plots to the equivalent simplified Randles circuit for the TRABs with different AEMs (Fig. S4). The membrane resistances were calculated by subtracting the solution resistance from the sum of the solution and membrane resistance (the left x-intercepts in the Nyquist plot).

increased with membrane thickness [23]. On average, the resistance of the B40-100 membrane appeared to be higher than that of the B40-150, but the difference was not significant (Student's t-test; $p = 0.15$). Similarly, the difference between the resistances of B25-100 and B25-150 was not significant ($p = 0.40$).

3.2. Power production of TRAB operated with different AEMs

Performance of the membranes was evaluated based on maximum power densities calculated from polarization tests. All three B40 membranes had power densities greater than those using the B25 or Selemion membranes. For each type of membrane, the maximum power density was inversely related to membrane thickness. For the B40 membranes, the maximum power density was 106 ± 7 W m^{-2} for the 50 μm thick membrane, and 89 ± 5 W m^{-2} for the 150 μm thick membrane. The same trend in power with membrane thickness was observed for B25 membranes. Lowering the IEC reduced the power production, where 95 ± 6 W m^{-2} was produced for the B40-100 membrane compared to 70 ± 4 W m^{-2} for the B25-100 membrane. Compared to the commercial Selemion membrane, power density could be increased by up to ~30% with the B40-50 membrane (Fig. 4a).

For all of the membrane samples, we examined whether the power densities were a significant function of the membrane resistance. The maximum power density significantly increased inversely with membrane resistance ($R^2 = 0.90$, $p < 0.01$) (Fig. 4b). Lowering the membrane resistance, which can be achieved by increasing the IEC or decreasing the thickness, facilitated the anion transfer rate through the AEM, resulting in a lower cell ohmic resistance and a higher power production.

3.3. Discharge/charge performance of TRAB with different AEM

In order to evaluate energy production of the TRABs using the different AEMs, electrical energy generation was examined over a complete discharge cycle, at the external resistance that produced the maximum power in the polarization test. For the fabricated membrane with a higher IEC (B40), the power was greater than that obtained using the Selemion membrane, with the battery fully discharged over a shorter period of time. When the IECs of the membrane were lower, for example for the B25-100 sample, the cell discharge time was similar to that obtained using a Selemion membrane (155 min for B25-100; 150 min for Selemion). However, in this case, the B25-100 system produced a higher power density compared to Selemion membrane. Increasing the membrane thickness slightly enhanced the discharge time. For example, the B40-50 TRAB was discharged for 110 min, while that of the B40-100 TRAB was 120 min (Fig. 5a).

The energy densities produced by the TRABs operated with B40-50 and B40-100 AEMs (high IEC) were lower than that obtained with the Selemion membrane. However, for the membranes with a lower IEC (i.e. B25), the energy densities were larger than that a TRAB with the Selemion membrane. The highest energy density obtained was 350 Wh m^{-3} using the B25-150 membrane, which was 13% higher than that with the Selemion membrane (Fig. 5b). Energy densities decreased with an increase in the IEC, although there was limited data for this comparison, but no significant relationship to the membrane resistance (Fig. 6).

The final catholyte pH increased with the membrane IEC. For example, after 90 min of cell discharge, pH of the catholyte for the

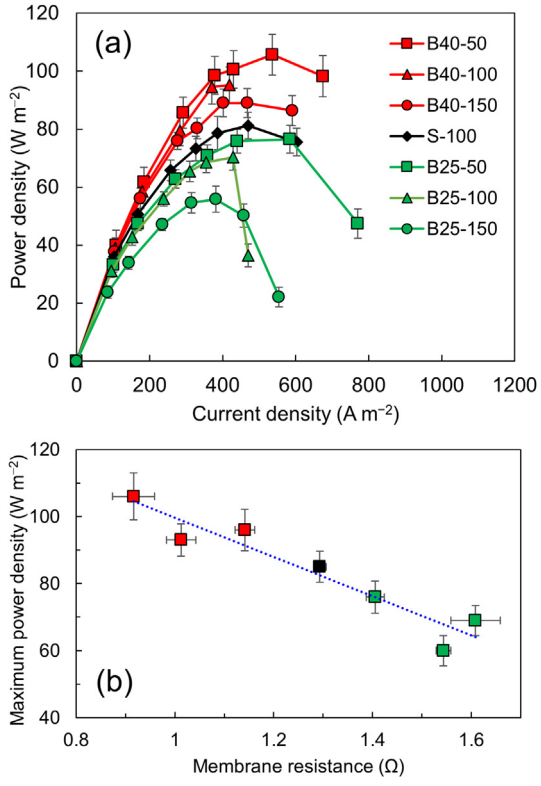

Fig. 4. (a) Power densities produced by TRABs operated with different AEMs, (b) maximum power density as a function of membrane resistance (red: B40s; black: Selemion; green: B25s). The data were well fitted to a linear regression model with a R^2 of 0.904, and a p-value (the significance of the slope) of less than 0.01. (For interpretation of the references to colour in this figure legend, the reader is referred to the web version of this article.)

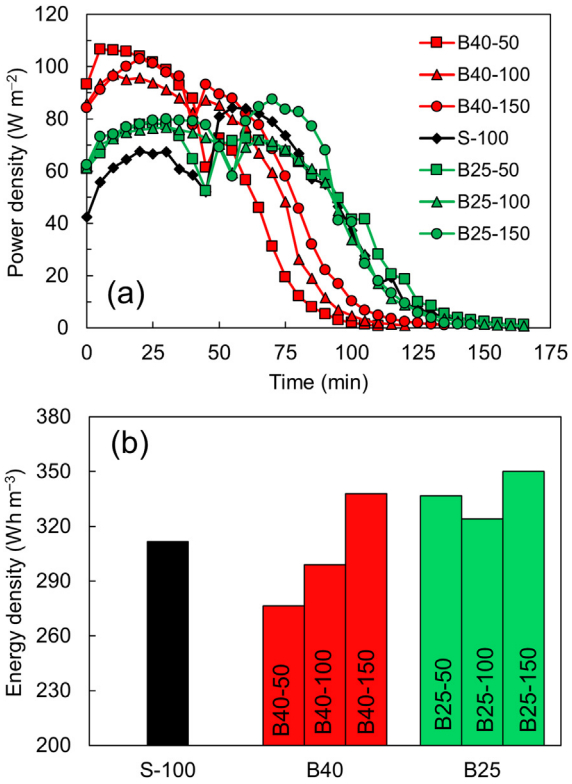

Fig. 5. (a) The discharge performance, (b) electrical energy density of TRABs with Selemion (S-100), B40, and B25 AEMs. The initial electrolyte contained 0.1 M Cu(II), 5 M NH_4NO_3, and the anolyte also contained 2 M NH_3. The sudden small drops on power density after 40–60 min was due to the anode replacement.

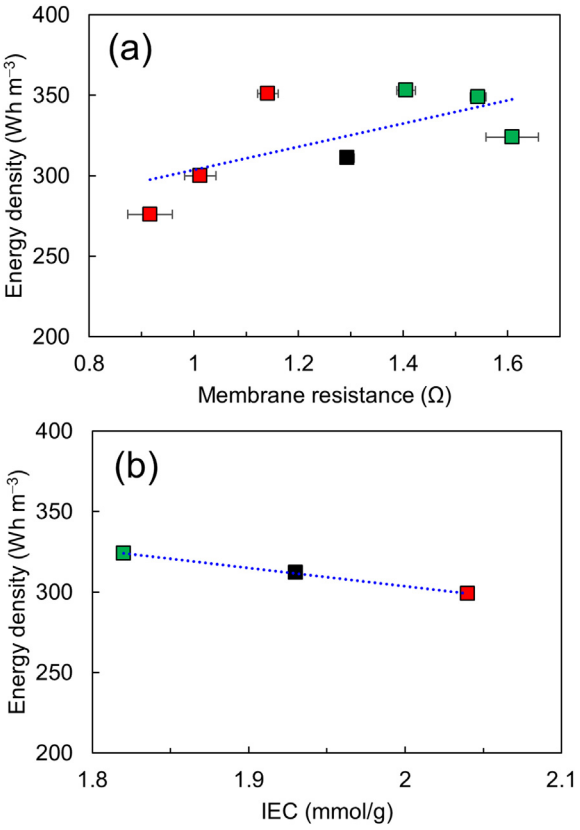

Fig. 6. TRAB energy density as a function of (a) membrane resistance with a R^2 of 0.417, (b) membrane IEC with a R^2 of 0.999, and a p-value of less than 0.01 (red: B40s; black: Selemion; green: B25s). The data showed the energy density was controlled by the membrane IEC and not the resistance. (For interpretation of the references to colour in this figure legend, the reader is referred to the web version of this article.)

TRAB with the B25-100 membrane increased from 2.6 to 6.5, while that for TRAB with the B40-100 membrane, the final pH increased to 7.1. This observation indicated that increasing the IEC likely enhanced the OH^- anion transfer rate through the AEM, resulting in a higher formation of NH_3 in the cathode chamber which led to an increased unfavorable chemical consumption of copper ions (Eqs. S2–S5) instead of the electrochemical depletion ($Cu^{2+} \rightarrow Cu^0$). Therefore, for a long experiment such as complete discharge to produce electrical energy, the benefit of a lower membrane resistance (i.e. a lower cell ohmic resistance) was likely offset by a higher IEC and greater crossover (i.e. a higher self-discharge rate).

The copper consumption with power generation, and the cathode coulombic efficiencies were measured to further investigate the impact of the membrane IEC on TRAB performance. The fabricated membrane with a higher IEC (B40) had the lowest copper electrochemical consumption of *CEC* = 47± 10%. The lowest *CEC* was obtained by the membrane with the highest IEC and the lowest thickness (B40-50; *CEC* of 29%). The *CEC* increased to 85%, which was 10% higher than for the Selemion sample, for the membrane with the lowest IEC and the greatest thickness (B25-150; Fig. 7). The *CCE*, which is the ratio of the produced current to the theoretical amount of current based on the change in mass of the cathode electrode, quantifies the relative importance of the Cu^{2+} electrodeposition reaction compared to other possible side electrochemical reactions [16,20]. A *CCE* of 67± 8% was achieved using the B40 (high IEC) AEMs, while the B25 membranes (low IEC) had a *CCE* of 97± 2%. The highest *CCE* of 98± 1% was obtained using the B25-100 membrane, which was 5% higher than the Selemion (Fig. 7).

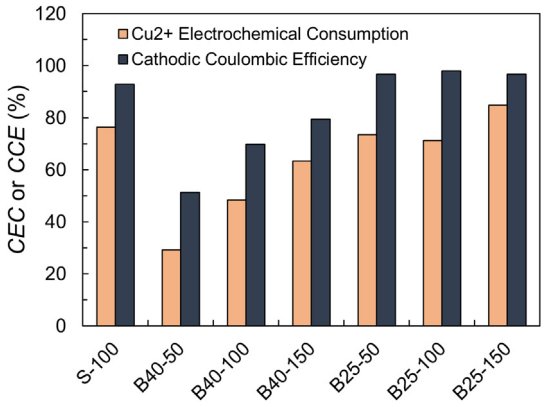

Fig. 7. Copper ion electrochemical consumption and cathodic coulombic efficiencies of TRABs with different AEMs.

The changes in the *CECs* and *CCEs* for different membranes can be understood by considering the impacts of the membrane IEC on ion transfer. Membranes with a higher IEC allow a higher transfer of OH^-, resulting in a higher formation of ammonia in the catholyte (Eq. S(1)). The formed ammonia can chemically consume Cu^{2+}, leading to a lowering of the *CEC* and TRAB performance in terms of energy density. In addition, using the B40-50 membrane (the highest IEC and the lowest thickness) would allow the highest OH^- transfer, and consequently, the highest rate of $Cu(NH_3)_4^{2+}$ formation in the cathode, resulting in $Cu(OH)_2$ blue precipitates due to the unwanted side reaction $Cu(NH_3)_4^{2+} + 4H_2O \rightarrow Cu(OH)_{2\ (s)} + 2\ NH_3 \cdot H_2O + 2\ NH_4^+$ [16]. The blue precipitates were visually observed just for the B40-50 membrane system, mainly due to a relatively high concentration of the formed $Cu(NH_3)_4^{2+}$. The positively charged copper amine complex can be also reduced according to the reactions 6 and 7, resulting in lowering of the *CCE* [35,36]. This improvement in the *CEC* and *CCE* by decreasing the IEC and increasing the thickness further explained the highest energy production of B25-150 AEM.

$$Cu(NH_3)_{4\ (aq)}^{2+} + e^- \rightarrow Cu(NH_3)_{4\ (aq)}^{+} \quad (6)$$

$$Cu(NH_3)_{4\ (aq)}^{2+} + e^- \rightarrow Cu(NH_3)_{2\ (aq)}^{+} + 2NH_{3\ (aq)} \quad (7)$$

3.4. Waste heat to electricity conversion efficiency

The thermal efficiency reflected the conversion efficiency of low grade waste heat as electrical power. In the TRAB, low grade waste heat (<130 °C) was used to recharge the battery by separating ammonia from the anolyte effluent and re-dissolving it in the catholyte. The heat required for electrolyte regeneration was evaluated based on the heat requirements for a distillation column with a reboiler temperature of 70.4 °C and condenser temperature of 43.3 °C, similar to our previous investigations [16,19,20]. Thermal efficiency followed the same trend as energy densities with respect to the thickness and IEC, with the highest efficiency of 0.97% for B25-150 (Table 2).

3.5. Comparison of performance with other systems

The maximum power densities achieved here varied from 55 W m^{-2} to 106 W m^{-2}-electrode was substantially higher than those obtained by the other waste heat-to-electricity systems

Table 2
Comparison of the thermal energy efficiency and that relative to the Carnot efficacy of the previously developed waste-heat-to-electricity systems, and the thermally regenerative battery assembled with Selemion or Bx (x = 25, 40) AEM.

System	Temperature difference (°C)	Efficiencies (%)		Reference
		Thermal	Relative to carnot	
Carbon multi-walled nanotube (MWNT) thermoelectrochemical cell	60	0.25	1.4	[37]
Carbon single-walled nanotube (SWNT)/reduced graphene oxide (rGO) composite electrode	31	NA	2.63	[38]
Carbon nanotube aerogel-based thermoelectrochemical cell	51	NA	3.95	[39]
Selemion-based TRAB	47	0.86	6.2	This study
B40-based TRABs	47	0.76–0.93	5.5–6.8	This study
B25-based TRABs	47	0.89–0.97	6.5–7.0	This study

(0.5–6.6 W m^{-2}) [37–39]. In addition, the TRAB with the B25-150 membrane was calculated to have a Carnot efficiency of 7.0%, which was higher than the Selemion TRAB (6.2%) and 1.8 times the highest previously reported value of 3.95% for a thermoelectrochemical cell operated with a 51 °C temperature difference between the carbon nanotube electrodes (Table 2) [39].

3.6. Synthesized membrane stability and durability

The acidic and alkaline stability of the fabricated membranes with different IEC were determined by polarization tests following immersion of the membranes in low pH catholyte or high pH anolyte solutions at room temperature. The results of the polarization tests for the acid soaked membranes showed 9% (B40) and 6% (B25) improvement in power production (Fig. 8a). For the alkaline stability tests, both membranes illustrated no significant change (<1% difference) in maximum power density, in good agreement with previous studies that have shown high alkaline stability of both the BTMA head group and the polymer backbone

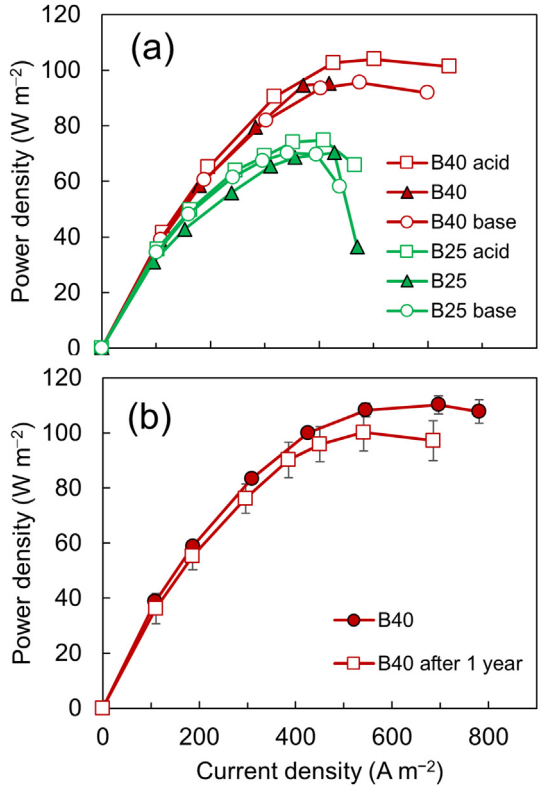

Fig. 8. Power densities of TRABs operated with (a) acid soaked, alkaline soaked AEMs with a thickness of 100 μm, (b) B40-50 AEM kept dry for a period of one year.

[40,41]. The durability of the BTMA-based membrane was also determined by storing a dry sample inside a constant temperature room for a period of one year. The polarization result showed that the maximum power density decreased less than 9% after one year, confirming that the fabricated membranes were durable in storage (Fig. 8b). In addition, no visual structural deformations, such as folding or cracking, were observed (Fig. S5).

4. Conclusions

TRAB performance in terms of power and energy density, and the overall waste heat-to-electricity conversion efficiency was enhanced by using a BTMA PPO-based AEM. An improvement of 31% in power density, and 13% in energy density was achieved using these new AEMs. The power density was primarily a function of the membrane resistance, while the energy density was a function of the membrane IEC. The TRAB with the fabricated membranes also showed a lower rate of cell self-discharge compared to the commercial Selemion membrane (11% enhancement). The overall thermal efficiency was ~1%, with a 7% efficiency relative to the Carnot efficiency for a TRAB operated with the B25-150 membrane.

Acknowledgments

The research was supported by awards from the National Science Foundation (CBET-1464891) and the European Copper Institute (WO 16038).

Appendix A. Supplementary data

Supplementary data related to this article can be found at http://dx.doi.org/10.1016/j.jpowsour.2017.01.003.

References

[1] S. Chu, A. Majumdar, Nature 488 (2012) 294–303.
[2] C. Forman, I.K. Muritala, R. Pardemann, B. Meyer, Renew. Sust. Energ. Rev. 57 (2016) 1568–1579.
[3] M.I. Hoffert, K. Caldeira, G. Benford, D.R. Criswell, C. Green, H. Herzog, A.K. Jain, H.S. Kheshgi, K.S. Lackner, J.S. Lewis, H.D. Lightfoot, W. Manheimer, J.C. Mankins, M.E. Mauel, L.J. Perkins, M.E. Schlesinger, T. Volk, T.M.L. Wigley, Science 298 (2002) 981–987.
[4] I. Johnson, T. William, W. Choate, A.A. Davidson, US Department of Energy, Office of Energy Efficiency and Renewable Energy, Industrial Technologies Program, Waste heat recovery: technology and opportunities in U.S. Industry, 2008.
[5] Y. Kim, J. Kim, S. Yamanaka, A. Nakajima, T. Ogawa, T. Serizawa, H. Tanaka, M. Baba, T. Fukuda, K. Yoshii, M. Takeda, N. Yamada, T. Nakayama, K. Niihara, Adv. Energy Mater. 5 (2015) 6.
[6] A.P. Straub, N.Y. Yip, S. Lin, J. Lee, M. Elimelech, Nat. Energy 1 (2016) 16090.
[7] A. Carati, M. Marino, D. Brogioli, Energy 93 (2015) 984–993. Part 1.
[8] X. Niu, J.L. Yu, S.Z. Wang, J. Power Sources 188 (2009) 621–626.
[9] S.B. Riffat, X.L. Ma, Appl. Therm. Eng. 23 (2003) 913–935.
[10] C. Amaral, C. Brandao, E.V. Sempels, F.J. Lesage, J. Power Sources 272 (2014) 672–680.
[11] L.E. Bell, Science 321 (2008) 1457–1461.
[12] E.H.B. Anari, M. Romano, W.X. Teh, J.J. Black, E. Jiang, J. Chen, T.Q. To,

J. Panchompoo, L. Aldous, Chem. Commun. 52 (2016) 745–748.
[13] M.A. Lazar, D. Al-Masri, D.R. MacFarlane, J.M. Pringle, Phys. Chem. Chem. Phys. 18 (2016) 1404–1410.
[14] X. Zhu, T. Kim, M. Rahimi, C. Gorski, B. Logan, ChemSusChem (2016), http://dx.doi.org/10.1002/cssc.201601220 (in press).
[15] T.I. Quickenden, Y. Mua, J. Electrochem. Soc. 142 (1995) 3985–3994.
[16] F. Zhang, J. Liu, W. Yang, B.E. Logan, Energy Environ. Sci. 8 (2015) 343–349.
[17] A.J. Bard, R. Parsons, J. Jordan, Standard Potentials in Aqueous Solution, Taylor & Francis, 1985.
[18] T. Kim, M. Rahimi, B.E. Logan, C.A. Gorski, ChemSusChem 9 (2016) 981–988.
[19] X. Zhu, M. Rahimi, C.A. Gorski, B. Logan, ChemSusChem 9 (2016) 873–879.
[20] F. Zhang, N. LaBarge, W. Yang, J. Liu, B.E. Logan, ChemSusChem 8 (2015) 1043–1048.
[21] M. Rahimi, Z. Schoener, X. Zhu, F. Zhang, C.A. Gorski, B.E. Logan, J. Hazard. Mater. 322 (2017) 551–556.
[22] J. Pan, L. Zhu, J.J. Han, M.A. Hickner, Chem. Mater. 27 (2015) 6689–6698.
[23] J.R. Varcoe, P. Atanassov, D.R. Dekel, A.M. Herring, M.A. Hickner, P.A. Kohl, A.R. Kucernak, W.E. Mustain, K. Nijmeijer, K. Scott, T.W. Xu, L. Zhuang, Energy Environ. Sci. 7 (2014) 3135–3191.
[24] N.W. Li, Y.J. Leng, M.A. Hickner, C.Y. Wang, J. Am. Chem. Soc. 135 (2013) 10124–10133.
[25] A.D. Mohanty, Y.B. Lee, L. Zhu, M.A. Hickner, C. Bae, Macromolecules 47 (2014) 1973–1980.
[26] L. Zhu, J. Pan, C.M. Christensen, B.C. Lin, M.A. Hickner, Macromolecules 49 (2016) 3300–3309.
[27] L. Zhu, J. Pan, Y. Wang, J. Han, L. Zhuang, M.A. Hickner, Macromolecules 49 (2016) 815–824.
[28] L. Zhu, T.J. Zimudzi, N. Li, J. Pan, B. Lin, M.A. Hickner, Polym. Chem. 7 (2016) 2464–2475.
[29] T. Kim, M. Rahimi, B.E. Logan, C.A. Gorski, Environ. Sci. Technol. 50 (2016) 9791–9797.
[30] X.T. Le, T.H. Bui, P. Viel, T. Berthelot, S. Palacin, J. Membr. Sci. 340 (2009) 133–140.
[31] X.T. Le, J. Colloid Interface Sci. 325 (2008) 215–222.
[32] C.X. Lin, Y.Z. Zhuo, A.N. Lai, Q.G. Zhang, A.M. Zhu, M.L. Ye, Q.L. Liu, J. Membr. Sci. 513 (2016) 206–216.
[33] G.M. Geise, M.A. Hickner, B.E. Logan, ACS Appl. Mater. Interfaces 5 (2013) 10294–10301.
[34] G.M. Geise, D.R. Paul, B.D. Freeman, Prog. Polym. Sci. 39 (2014) 1–42.
[35] F. Habashi, Ber. Bunsen Ges. Phys. Chem. 67 (1963) 402–406.
[36] D. Grujicic, B. Pesic, Electrochim. Acta 50 (2005) 4426–4443.
[37] R. Hu, B.A. Cola, N. Haram, J.N. Barisci, S. Lee, S. Stoughton, G. Wallace, C. Too, M. Thomas, A. Gestos, M.E.d. Cruz, J.P. Ferraris, A.A. Zakhidov, R.H. Baughman, Nano Lett. 10 (2010) 838–846.
[38] M.S. Romano, N. Li, D. Antiohos, J.M. Razal, A. Nattestad, S. Beirne, S. Fang, Y. Chen, R. Jalili, G.G. Wallace, R. Baughman, J. Chen, Adv. Mater 25 (2013) 6602–6606.
[39] H. Im, T. Kim, H. Song, J. Choi, J.S. Park, R. Ovalle-Robles, H.D. Yang, K.D. Kihm, R.H. Baughman, H.H. Lee, T.J. Kang, Y.H. Kim, Nat. Commun. 7 (2016).
[40] D. Chen, M.A. Hickner, ACS Appl. Mater. Interfaces 4 (2012) 5775–5781.
[41] H. Long, K. Kim, B.S. Pivovar, J. Phys. Chem. C 116 (2012) 9419–9426.